## Title

D-peptide-magnetic nanoparticles fragment tau fibrils and rescue behavioral deficits in a mouse model of Alzheimer's disease



## Journal

Science Advances, 10(18)

## ISSN

2375-2548

## Authors

Hou, Ke
Pan, Hope
Shahpasand-Kroner, Hedieh
et al.

## Publication Date

2024-05-01

## DOI

10.1126/sciadv.adl2991

Peer reviewed

BIOCHEMISTRY

# D-peptide-magnetic nanoparticles fragment tau fibrils and rescue behavioral deficits in a mouse model of Alzheimer's disease

**Ke Hou[1,2,3,4,5], Hope Pan[1,2,3,4,5], Hedieh Shahpasand-Kroner[6,7,8], Carolyn Hu[1,2,3,4,5], Romany Abskharon[1,2,3,4,5], Paul Seidler[1,2,3,4,5,9], Marisa Mekkittikul[6,7,8], Melinda Balbirnie[1,2,3,4,5], Carter Lantz[1], Michael R. Sawaya[1,2,3,4], Joshua L. Dolinsky[1,2,3,4,5], Mychica Jones[6,7,8], Xiaohong Zuo[6,7,8], Joseph A. Loo[1,2,3,4], Sally Frautschy[6,7,8], Greg Cole[6,7,8], David S. Eisenberg[1,2,3,4,5]***



**Amyloid fibrils of tau are increasingly accepted as a cause of neuronal death and brain atrophy in Alzheimer's disease (AD). Diminishing tau aggregation is a promising strategy in the search for efficacious AD therapeutics. Previously, our laboratory designed a six-residue, nonnatural amino acid inhibitor D-TLKIVW peptide (6-DP), which can prevent tau aggregation in vitro. However, it cannot block cell-to-cell transmission of tau aggregation. Here, we find D-TLKIVWC (7-DP), a D-cysteine extension of 6-DP, not only prevents tau aggregation but also fragments tau fibrils extracted from AD brains to neutralize their seeding ability and protect neuronal cells from tau-induced toxicity. To facilitate the transport of 7-DP across the blood-brain barrier, we conjugated it to magnetic nanoparticles (MNPs). The MNPs-DP complex retains the inhibition and fragmentation properties of 7-DP alone. Ten weeks of MNPs-DP treatment appear to reverse neurological deficits in the PS19 mouse model of AD. This work offers a direction for development of therapies to target tau fibrils.**



## INTRODUCTION

Alzheimer's disease (AD) is a progressive and fatal neurodegenerative disorder characterized by two major neuropathologic hallmarks: extracellular senile plaques containing fibrils of amyloid beta (Aβ) and intracellular neurofibrillary tangles of tau (*1*). Increasing evidence indicates that cognitive symptoms and severity in AD are more strongly correlated with tau pathology than Aβ plaques (*2*). The failure of multiple phase 3 clinical trials with Aβ-targeting drugs (*3*) has redirected AD therapeutics to focus on targeting tau pathology. Researchers have pursued diverse approaches to diminish tau aggregation in AD, including reducing expression of the *MAPT* gene which encodes tau, modulating posttranslational modifications of tau, preventing tau aggregation, passive antibody immune neutralization, or clearance of different tau species, and stabilizing the microtubules to which tau binds (*4*). So far, tau antibodies have failed in the clinic (*5*), possibly due to their inability to penetrate neurons. Tau aggregation inhibitors such as curcumin and methylene blue/LMTX have progressed to phase 2 and phase 3 clinical trials, respectively, but have yet to show efficacy in treating disease (*4*). These molecules fell short partly due to their limited biocompatibility (*6*) and low blood-brain barrier (BBB) permeability (*7*). Recently, nanomaterials applied as drug candidates or drug carriers have been reported to overcome these limitations (*8*). Among them, magnetic nanoparticles (MNPs) have attracted attention as magnetic resonance imaging contrast agents and drug carriers in AD (*9*). MNPs are benign, easily functionalized, and able to cross the BBB.

To diminish tau aggregation, our laboratory has developed structure-based design of compounds aimed to inhibit tau aggregation or disassemble tau fibrils (*10*–*12*). For example, Sievers *et al.* (*10*) used the atomic structure of a segment from the tau fibril core as a template to design a six-residue, nonnatural amino acid inhibitor D-TLKIVW peptide (6-DP) that binds the ends of tau fibrils to cap their growth; 6-DP was demonstrated to prevent tau aggregation in vitro. Compared to L-enantiomeric peptides, D-enantiomeric peptides are known to be less immunogenic, less protease-sensitive in vitro, and more resistant to degradation in vivo (*13*). While D-TLKIVW inhibits fibril growth, it does not prevent AD-extracted tau seed spreading in biosensor cells (*14*) and is theoretically unable to cross the BBB, which limits its clinical potential.

Here, we designed a seven-residue D-TLKIVWC peptide (7-DP), which is a C-terminal D-cysteine extension of D-TLKIVW. We found 7-DP to be a better inhibitor of tau fibril growth than 6-DP in vitro and in addition to be a tau fragmentor. To facilitate its transport across the BBB and improve its stability, we conjugated 7-DP with MNPs. We found the treatment of 7-DP–conjugated MNPs (MNPs-DP) reversed the behavioral deficits of PS19 mice, a model of AD tauopathy. 7-DP not only prevents tau aggregation but also dissolves existing tau aggregates.

[1]Department of Chemistry and Biochemistry, UCLA, Los Angeles, CA, USA. [2]Department of Biological Chemistry, UCLA, Los Angeles, CA, USA. [3]UCLA-DOE Institute, Los Angeles, CA, USA. [4]Molecular Biology Institute, UCLA, Los Angeles, CA, USA. [5]Howard Hughes Medical Institute, Los Angeles, CA, USA. [6]Department of Neurology, UCLA, Los Angeles, CA, USA. [7]Veterans Administration Greater Los Angeles Healthcare System, Geriatric Research and Clinical Core, Los Angeles, CA, USA. [8]Department of Medicine, UCLA, Los Angeles, CA, USA. [9]Department of Pharmacology and Pharmaceutical Sciences, University of Southern California, Los Angeles, CA, USA.
*Corresponding author. Email: david@mbi.ucla.edu

## RESULTS

### D-TLKIVWC is a better inhibitor of tau aggregation than D-TLKIVW

We first evaluated D-TLKIVWC (7-DP) as an inhibitor of tau aggregation by comparing its effects on fibril formation of tau $K18^+$ to that of the previously published inhibitor D-TLKIVW (6-DP) (*10*). $K18^+$ is a recombinant construct of tau, spanning residues 244 to

380, which forms the ordered core visible in the cryo–electron microscopy structure of tau fibrils extracted from postmortem brains of patients with AD (*15*). The aggregation kinetics of tau K18$^+$ monomer incubated alone or with increasing concentrations of 7-DP or 6-DP were monitored by thioflavin T (ThT) assays in parallel. Tau K18$^+$ fibrillation exhibited typical sigmoidal curves (black line in Fig. 1A and fig. S1A); both 7-DP (Fig. 1A) and 6-DP (fig. S1A) showed dose-dependent inhibition of tau K18$^+$ aggregation by prolonging the lag phase and decreasing the ThT fluorescence signal. However, 7-DP is a stronger inhibitor than 6-DP because its estimated median inhibitory concentration ($IC_{50}$) is 12.1 ± 0.3 μM (fig. S1B) compared to that of 19.6 ± 1.4 μM (fig. S1C) for 6-DP. Consistent with these results, in parallel circular dichroism (CD) spectroscopy further revealed that 7-DP can better prevent tau K18$^+$ monomers from forming β sheet structures (probed by the negative peak around 220 nm) and keep tau in a random coil conformation with a negative peak near 200 nm (fig. S1, D and E). Transmission electron microscopy (TEM) showed the counts and length of tau K18$^+$ fibrils decreased with the increased dose of 7-DP or 6-DP (fig. S2), but 7-DP reduced the abundance of fibrils more than 6-DP, especially at 100 μM concentration, where no tau K18$^+$ fibrils (red arrows) were observed; only tau oligomers (black arrows) and fibrils formed from 7-DP itself (blue arrow) were seen. Together, these data show that D-TLKIVWC is a better tau fibril-binding inhibitor than D-TLKIVW.

## D-TLKIVWC fragments recombinant tau K18$^+$ fibrils

To characterize its fragmentation ability, we added 7-DP to preformed tau K18$^+$ fibrils and observed an immediate decrease in ThT fluorescence intensity, whereas adding $H_2O$ or 6-DP had no notable effect on the ThT signal (Fig. 1B). TEM characterization revealed that incubation of preformed tau K18$^+$ fibrils with 7-DP led to the disappearance of tau fibrils and the appearance of globular species, whereas 6-DP could not change the morphology of tau K18$^+$ fibrils (Fig. 1C). After incubation with 7-DP, we observed a slight shift in the broad peak of tau fibrils (shown by the blue dashed line in fig. S3) toward lower mass/charge ratio in their native electrospray ionization mass spectra, suggesting that the fibrils were fragmented

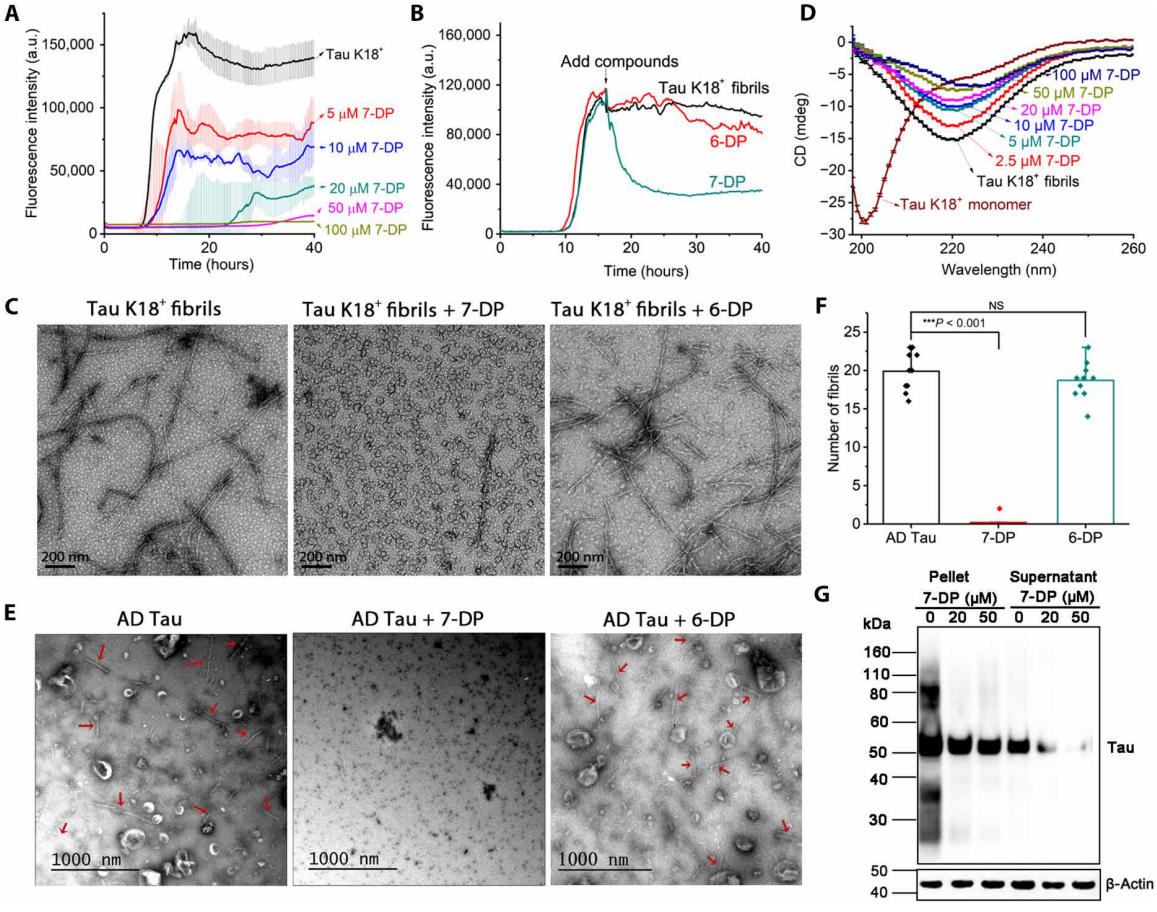


**Fig. 1. 7-DP inhibits tau aggregation and fragments tau fibrils in vitro and in cells.** (**A**) ThT assays of 20 μM tau K18$^+$ monomer incubated alone or in the presence of 5, 10, 20, 50, and 100 μM 7-DP. (**B**) ThT fragmentation assay of 20 μM tau K18$^+$ fibrils with $H_2O$, 50 μM 6-DP, or 50 μM 7-DP added at 16 hours. (**C**) TEM image of 20 μM recombinant tau K18$^+$ fibrils before and after 24 hours of incubation with 50 μM 7-DP or 50 μM 6-DP at 37°C. Scale bars, 200 nm. (**D**) CD spectra of tau K18$^+$ monomer, tau K18$^+$ fibrils before and after incubation with various concentrations of 7-DP for 48 hours at 37°C. (**E**) Representative TEM images of AD-extracted tau fibrils (indicated by red arrows) before and after 48 hours of incubation with 500 μM 7-DP or 500 μM 6-DP at 37°C. (**F**) Quantification of AD tau fibrils in TEM images ($n$ = 10 images). (**G**) Western blotting analysis of cell lysate from HEK293 cells expressing 1N4R tau treated with 20 μM or 50 μM 7-DP, using Dako tau antibody. β-Actin was used as a loading control. a.u., arbitrary units.

by 7-DP. To further verify that 7-DP can fragment tau K18$^+$ fibrils, a dose-dependent experiment was performed. As expected, 7-DP treatment caused a dose-dependent decrease of (i) β strand content of tau K18$^+$ fibrils as measured by CD spectroscopy (Fig. 1D), (ii) ThT fluorescence intensity (fig. S4A), (iii) binding of the anti-amyloid OC antibody (fig. S4B), and (iv) number of tau K18$^+$ fibrils under TEM (fig. S4, C to I). It was noteworthy that the globular species in Fig. 1C and fig. S4I was significantly larger than tau oligomers observed in fig. S2A (fig. S4J), indicating that the fragmented products of tau fibrils by 7-DP were probably the tau K18$^+$ and 7-DP complex. Collectively, these data establish that 7-DP can fragment recombinant tau K18$^+$ fibrils, whereas 6-DP cannot. The fragmented products were probably composed of tau K18$^+$ and 7-DP.

### D-TLKIVWC fragments AD-extracted tau fibrils

Previous studies have revealed that heparin-induced recombinant tau K18$^+$ fibrils adopt different structures than pathological tau fibrils in AD (*16*). Here, we investigated whether 7-DP can fragment tau fibrils extracted from autopsied AD brains (AD tau fibrils) (*17*). TEM characterization showed that most of the AD tau fibrils disappeared after incubation with 500 μM 7-DP for 2 days, while abundant AD tau fibrils remained in the 6-DP–treated sample (Fig. 1E). Quantification confirmed that 7-DP significantly reduced the number of AD tau fibrils, but 6-DP did not (Fig. 1F). To further verify that 7-DP can fragment AD tau fibrils, we incubated AD tau fibrils with various concentrations of 7-DP. After 48 hours, a dot blot experiment was performed with the monoclonal antibody GT38, which specifically recognizes AD tau fibrils. The dose-dependent decrease of chemiluminescence intensity in fig. S5 (A and B) indicated that 7-DP reduced the amount of AD Tau fibrils in a dose-dependent manner. Western blotting of the supernatant and pellet of AD tau fibrils before and after 48 hours of incubation with 7-DP indicated that the fragmented products were not soluble tau monomers; instead, they were a series of insoluble species, containing dimers and other degraded fragments (fig. S5C).

### D-TLKIVWC fragments tau aggregates in cells

As 7-DP is able to fragment recombinant and AD-extracted tau fibrils, we tested whether 7-DP could fragment intracellular tau aggregates. We expressed 1N4R tau in human embryonic kidney (HEK) 293 cells and seeded them with AD-extracted tau fibrils for 24 hours to accumulate tau aggregates. The successful formation of tau aggregates in the cell was confirmed by Western blot in fig. S5D, where AD tau-seeded group showed more tau contents in the pellet compared with nonseeded group. The cells were then transfected with 7-DP followed by a 24-hour incubation, before lysis and ultracentrifugation. Tau content in the pellet and supernatant was analyzed by Western blot using antitau rabbit polyclonal antibody (Dako, A0024). The result showed that the 7-DP reduced the tau content in both the pellet and supernatant in a 7-DP dose-dependent manner (Fig. 1G). Cotreatment with proteasome inhibitor MG132 reduced the effect of 7-DP, indicating that the tau was possibly degraded by the ubiquitin-proteasome pathway (fig. S5D) (*18*). Whether tau is degraded alone or in a 7-DP–tau complex remains to be determined. In addition, we used another HEK293T cell line stably expressing enhanced yellow fluorescent protein (EYFP)–fused tau 1N4R P301S to visualize whether 7-DP could fragment tau aggregates in cells. Similarly, we first transfected AD tau fibril seeds to induce the aggregation of the endogenous fluorescent tau, which formed bright puncta visible under fluorescence microscopy (indicated by white arrows in fig. S5E). The introduction of 7-DP later significantly decreased the number of puncta compared with phosphate-buffered saline (PBS)–treated group (fig. S5, E and F). These experiments indicated that 7-DP can fragment tau aggregates in cells.

### D-TLKIVWC blocks AD-extracted tau seeding in tau biosensor cells

It has been suggested that tau pathology propagates through the brain following a prion-like mechanism, in which aggregates in a diseased cell can travel to adjacent cells and seed further protein aggregation (*19*, *20*). Blocking the prion-like spread of tau may halt the progression of AD. We used a HEK293T cell line stably expressing yellow fluorescent protein (YFP)–fused tau (tau biosensor cell) to investigate whether 7-DP could block the spread of tau pathology (*21*). We transfected AD tau fibril seeds to induce the aggregation of the endogenous fluorescent tau, which formed bright puncta visible by fluorescence microscopy (indicated by white arrows in Fig. 2A). Automated image analysis of visible puncta provided an objective quantification of seeded aggregation (Fig. 2B). When AD tau fibrils were incubated with 7-DP overnight before transfection, tau puncta were reduced significantly with an $IC_{50}$ of 7-DP around 33.5 μM (Fig. 2, A and B). We also tested whether 7-DP could block AD-extracted tau seeding when 7-DP and AD tau seeds were directly transfected to biosensor cells without preincubation overnight. 7-DP showed comparable performance in blocking tau spreading [fig. S6 (A and B) versus Fig. 2 (A and B)]. This reduction suggested the inhibition and fragmentation capacity of 7-DP, which can change or destroy the structure of AD tau fibrils and render them no longer seeding competent. Consistent with our previous report (*14*), 6-DP had no measurable inhibition of AD-extracted tau seeding with concentrations up to 100 μM (fig. S6, C to E).

### D-TLKIVWC protects neuronal cells from tau-induced toxicity

Next, we investigated the ability of 7-DP to protect neurons from tau-induced toxicity. The 3-(4,5-dimethylthiazol-2-yl)-2,5-diphenyl tetrazolium bromide (MTT) metabolic assay showed that Neuro2a (N2a) cells exposed to tau K18$^+$ aggregates, formed by tau K18$^+$ monomer incubated alone, had a significantly reduced cell viability of ~35% (Fig. 2C). In contrast, the aggregates of tau K18$^+$ and 7-DP significantly increased cell viability of N2a cells with median effective concentration ($EC_{50}$) of 7-DP around 21.1 μM (Fig. 2C). This indicated that 7-DP can protect neuronal cells from tau-induced toxicity by inhibiting tau aggregation. 6-DP also showed a slight improvement in cell viability, but it was not as effective as 7-DP (fig. S7A) and an estimate of $EC_{50}$ was unobtainable.

We performed another MTT assay by treating N2a cells with preformed tau K18$^+$ fibrils. Incubation of tau K18$^+$ fibrils with 7-DP gave rise to higher cell viability compared with tau K18$^+$ fibrils alone (Fig. 2D), indicating that unlike putative toxic tau oligomers, the fragmented products of tau K18$^+$ fibrils by 7-DP were nontoxic or less toxic than tau fibrils. As expected, 6-DP did not reduce the cytotoxicity of tau fibrils (fig. S7B), presumably because it cannot disassemble tau fibrils. Both 7-DP (Fig. 2E) and 6-DP (fig. S7C) alone were nontoxic to N2a cells under all tested concentrations.

### Conjugation of MNPs-DP complex

Encouraged by the inhibition and fragmentation properties of 7-DP, we aimed to evaluate its clinical potential in vivo. However, 7-DP is

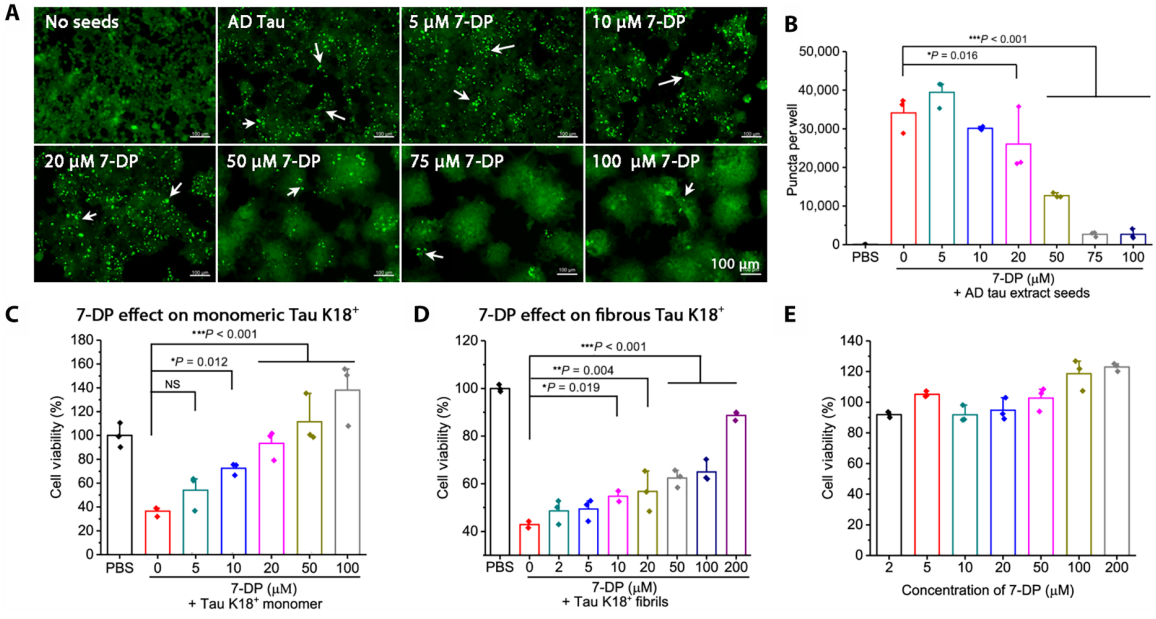


**Fig. 2. 7-DP blocks tau seeding and reduces tau-induced cell toxicity.** (**A**) Representative fluorescent images of HEK293 cells expressing YFP-labeled tau K18 transfected with AD tau fibril seeds in various concentrations of 7-DP. Fluorescent puncta were marked by white arrows. Scale bars, 100 μm. (**B**) Quantification of puncta formed in tau biosensor cells seeded with AD tau fibrils with various concentrations of 7-DP. (**C**) Cell viability of N2a cells treated with tau K18$^+$ monomer incubated alone or in various concentrations of 7-DP, measured by MTT assay. 7-DP treatment of tau K18$^+$ monomer rescues cell viability. (**D**) Cell viability of N2a cells treated with tau K18$^+$ fibrils in various concentrations of 7-DP, measured by MTT assay. 7-DP treatment of tau K18$^+$ fibrils rescues cell viability. (**E**) N2a cells treated with a range of 7-DP concentrations shows no toxicity. Results shown as mean + SD of triplicate wells. Statistical significance was analyzed by one-way analysis of variance (ANOVA) (*$P < 0.05$; **$P < 0.01$; ***$P < 0.001$; NS, not significant).

likely to have poor BBB permeability and structural stability due to its large mass (>800 Da) and the active sulfhydryl group in its side chain. To address these challenges, we conjugated 7-DP to MNPs, which have been approved for clinical use (*22*) and are reported to be stable, benign, and able to cross the BBB (*23*). The conjugation involves two steps (fig. S8). Briefly, the carboxylic acid-stabilized iron oxide MNPs (CD Bioparticles, WHM-G062) were functionalized with a maleimide group (MNPs-MAL) and then covalently bonded to the sulfhydryl group of 7-DP through the thiol-maleimide Michael addition click reaction (*24*). Successful conjugation between MNPs and 7-DP was confirmed by morphological changes (from dispersed to aggregated and then dispersed) observed with TEM (fig. S9, A to C), a notable increase of hydrodynamic size and reduction of zeta potential measured by dynamic light scattering (fig. S9D). The conjugation efficiency of 7-DP to MNPs was ~94% estimated by the ultraviolet absorbance spectrum of 7-DP (fig. S10). This implied that the concentration of 7-DP on the MNP surface was ~4.3 mM/mg of MNPs.

## MNPs-DP show a dose-dependent inhibition of tau K18$^+$ aggregation

ThT assay (Fig. 3A) and TEM characterization (Fig. 3B and fig. S11) demonstrated that like 7-DP, MNPs-DP inhibited tau K18$^+$ aggregation and reduced the length of tau fibrils in a dose-dependent manner. To rule out the possibility that the inhibition of MNPs-DP originated from the MNPs or the conjugation process, naked MNPs and a scrambled peptide D-LKTWIVC–conjugated MNPs (MNPs-DPsc) were tested following the same aggregation protocols. Neither naked MNPs (fig. S12) nor MNPs-DPsc (fig. S13) prevented tau aggregation, indicating that MNPs-DP retained the specificity of 7-DP in inhibiting tau aggregation.

## MNPs-DP fragment recombinant tau K18$^+$ fibrils and AD-extracted tau fibrils

In addition to inhibiting tau K18$^+$ aggregation, MNPs-DP also fragmented preformed tau K18$^+$ fibrils as evidenced by the decrease of ThT signal (Fig. 3C), as well as by the reduction of tau K18$^+$ fibrils and the appearance of globular species under TEM (fig. S14, A and B). However, MNPs-DP (83 μM DP, red line in Fig. 3C) did not work as efficiently as 7-DP (50 μM, blue line in Fig. 3C) to fragment tau K18$^+$ fibrils (Fig. 3C and fig. S14, B and C). This result is reasonable, considering that conjugation of 7-DP onto the surface of MNPs may limit the geometry of interaction between 7-DP and tau K18$^+$ fibrils. Fragmentation of tau K18$^+$ fibrils by MNPs-DP was verified to be dose dependent via (i) reduction of ThT fluorescence intensity (Fig. 3D), (ii) decrease of binding to anti-amyloid OC antibody (fig. S15A), and (iii) reduction of the abundance of tau K18$^+$ fibrils and a concurrent increase in the number of globular species observed by TEM (Fig. 3E and fig. S15, B and C). MNPs-DP fragmented AD-extracted tau fibrils after a 48-hour incubation (Fig. 3, F and G). In contrast, the naked MNPs alone could not disassemble tau K18$^+$ fibrils (Fig. 3C and fig. S14D) or AD tau fibrils at any dose (Fig. 3, F and G).

## MNPs-DP block AD-extracted tau seeding in tau biosensor cells

After incubating AD tau fibril seeds with MNPs-DP overnight and then transfecting them into tau biosensor cells, we observed a

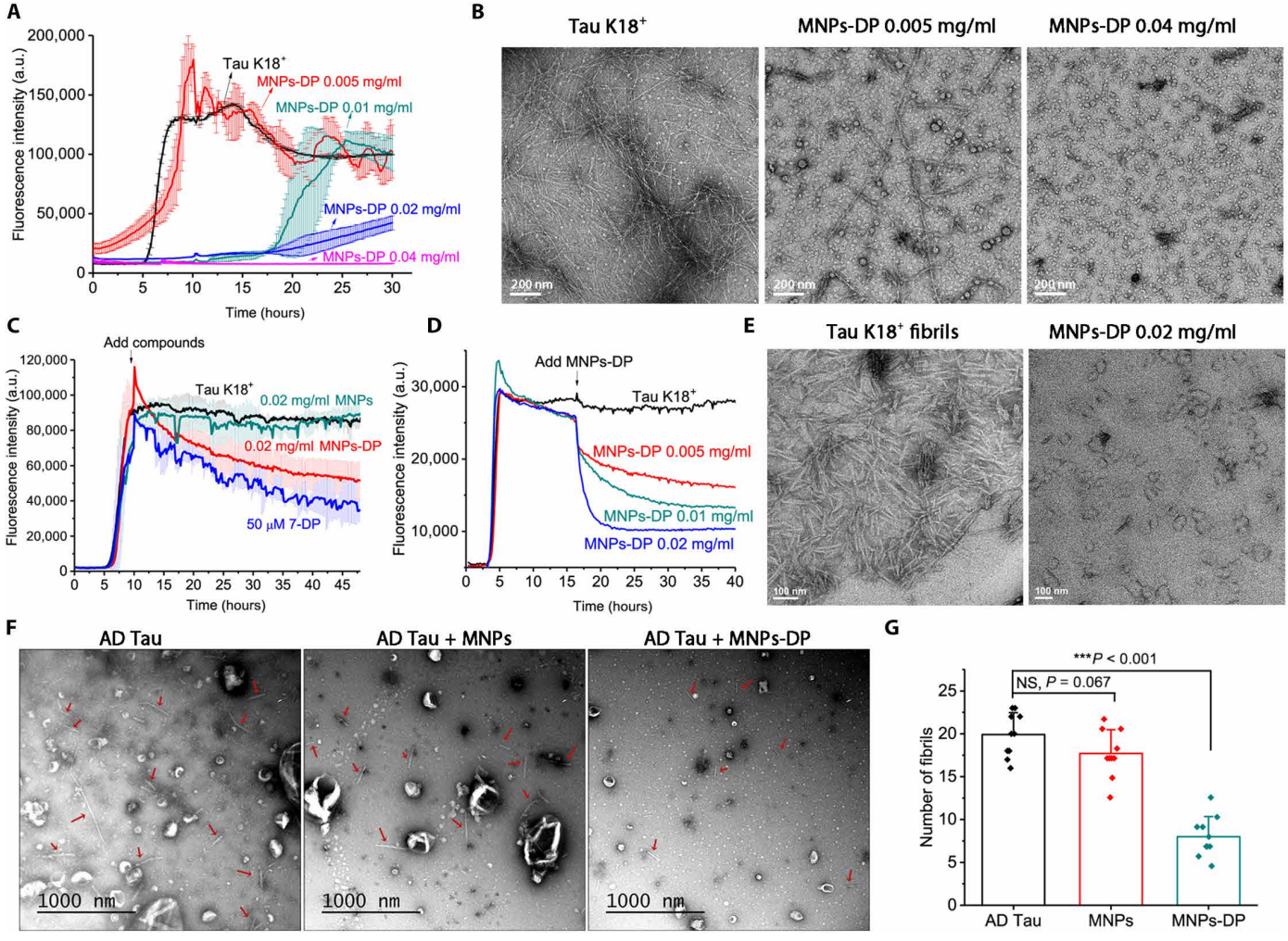


**Fig. 3. MNPs-DP retain the properties of 7-DP to inhibit tau aggregation and fragment tau fibrils in vitro.** (**A**) ThT assays of 20 μM tau K18$^+$ monomer incubated alone or in the presence of MNPs-DP (0.005, 0.01, 0.02, and 0.04 mg/ml). The concentration of 7-DP on the surface of MNPs is 21.5, 43, 86, 172 μM, respectively. (**B**) TEM images of tau K18$^+$ incubated alone or in the presence of MNPs-DP (0.005 and 0.04 mg/mL) for 48 hours. Scale bars, 200 nm. (**C**) ThT fragmentation assay of 20 μM tau K18$^+$ fibrils with $H_2O$, MNPs (0.02 mg/ml), MNPs-DP (0.02 mg/ml; 86 μM 7-DP), or 50 μM 7-DP added at 10 hours. (**D**) ThT fragmentation assay of 20 μM tau K18$^+$ fibrils with MNPs-DP (0.005, 0.01, and 0.02 mg/ml) added at 16 hours. (**E**) TEM images of tau K18$^+$ fibrils before and after 24 hours of incubation with MNPs-DP (0.02 mg/ml). Scale bars, 100 nm. (**F**) Representative TEM images of AD-extracted tau fibrils (indicated by red arrows) before and after 48 hours of incubation with MNPs (0.02 mg/ml) or MNPs-DP (0.02 mg/ml; 86 μM 7-DP) at 37°C. (**G**) Quantification of AD tau fibrils in TEM images ($n$ = 10 images).

dose-dependent reduction in the number of tau puncta (Fig. 4, A and B). The $IC_{50}$ was calculated to be 0.0067 mg/ml MNPs-DP (28.9 μM 7-DP), which is slightly better than that of 7-DP alone (33.5 μM; Fig. 2, A and B). This improvement may be attributed to the enhanced stability of 7-DP on the MNP surface, which protects it from intracellular proteases and the complex redox environment within cells. Our results suggest that, like free 7-DP, MNPs-DP can inhibit the prion-like propagation of tau pathology by capping and fragmenting AD tau fibrils. In contrast, the naked MNPs had no effect on preventing tau seeding in tau biosensor cells (fig. S16).

## MNPs-DP reduce tau-induced cell toxicity

We used MTT assays to show that MNPs-DP can protect N2a neuronal cells from tau-induced toxicity by inhibiting tau K18$^+$ aggregation (Fig. 4C) and fragmenting tau K18$^+$ fibrils (Fig. 4D). MNPs-DP alone were nontoxic to N2a cells under all tested concentrations (fig. S17A). Our control MNPs were found to be harmless, as previously reported (fig. S17B) (*23*) but had no effect on reducing tau-induced cell toxicity (fig. S17, C and D).

## MNPs-DP cross the BBB in C57BL/6J mice

To assess the ability of MNPs-DP to penetrate the BBB, we administered MNPs-DP (10 mg/kg body weight) to 2-month-old wild-type (WT) C57BL/6J mice via tail vein injection, following intranasal injection of 20 μl of 2% mannitol. After 2 hours, the mice were euthanized, and their brains were perfused to wash out residual MNPs-DP from the blood vessels. We analyzed the Fe levels in the brain by inductively coupled plasma mass spectrometry (ICP-MS) after digesting the brain tissues. We observed a 1.5-fold increase in estimated Fe concentration in the brains of mice that were injected with MNPs-DP compared to PBS-injected mice ($n$ = 3 per group; fig. S18), suggesting that MNPs-DP can cross the BBB.

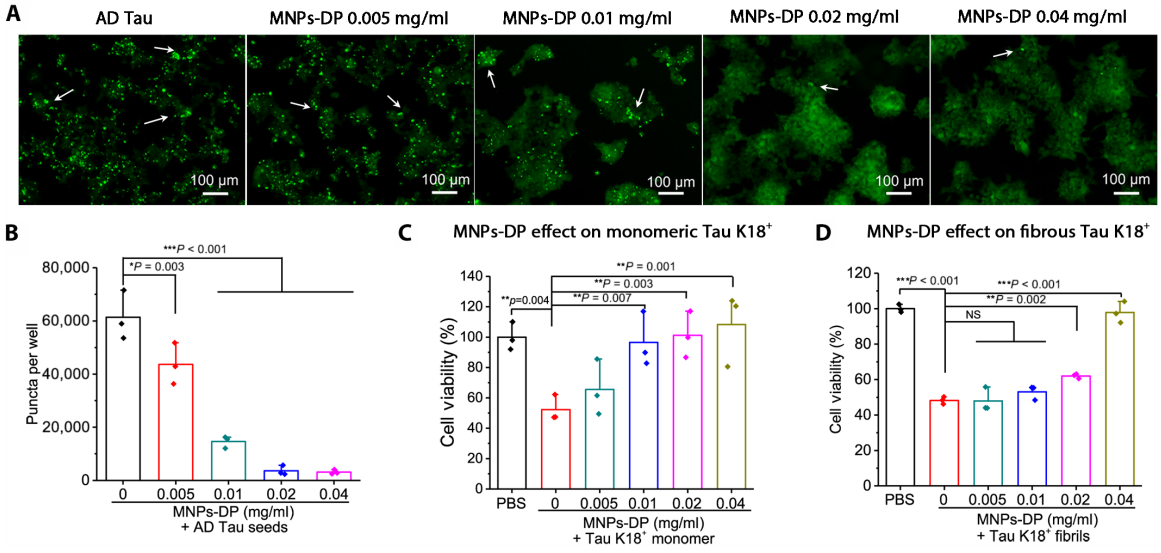


**Fig. 4. MNPs-DP block tau seeding and reduce tau-induced cell toxicity in cells.** (**A**) Representative fluorescence images of HEK293 cells expressing YFP-labeled tau K18 transfected with AD tau fibril seeds in various concentrations of MNPs-DP. Fluorescent puncta were marked by white arrows. Scale bars, 100 μm. (**B**) Quantification of puncta formed in tau biosensor cells seeded with AD tau fibrils in various concentrations of MNPs-DP. (**C**) Cell viability of tau K18$^+$ monomer incubated alone or in various concentrations of MNPs-DP, assessed by MTT assay. (**D**) Cell viability of N2a cells treated with tau K18$^+$ fibrils, in various concentrations of MNPs-DP measured by MTT assay. Results shown as mean + SD of triplicate wells. Statistical significance was analyzed by one-way ANOVA (*$P$ < 0.05; **$P$ < 0.01; ***$P$ < 0.001).

## MNPs-DP rescue memory deficits of the PS19 mouse model of AD

We used the PS19 transgenic mice that overexpress the P301S mutant form of human microtubule-associated protein tau (*MAPT*) (*25*) as a tauopathy model to investigate the therapeutic efficiency of MNPs-DP against AD-related tauopathy in vivo, although the structures of tau filaments from PS19 mice differ from those of WT tau filaments from human brains (*26*). Two-month-old male PS19 mice were stereotaxically injected with tau K18$^+$ fibril seeds to induce similar and consistent levels of tau pathology in cohorts of PS19 mice (*27*). Similarly, 6-month-old female PS19 mice were also seeded and adopted as a second cohort of PS19 mice. Two weeks after the stereotaxic surgery, MNPs-DP, MNPs, and vehicle (PBS) were tail vein–injected into PS19 transgenic mice weekly for 10 weeks at a dose of 10 mg/kg of body weight ($n$ = 13 per group, eight male and five female mice for each group). WT, age-matched control C57BL/6J mice also received identical stereotaxic surgery but were injected with vehicle (PBS) as controls for surgery, injection, and anesthesia. The body weights of mice were recorded weekly, and MNPs-DP significantly prevented weight loss of PS19 mice associated with late-stage tau pathology that afflicted vehicle- or naked MNP-treated PS19 mice after 10 weeks of treatment (Fig. 5A). At the end of the 10-week treatment, we assessed the spatial cognition and memory of these mice using the Barnes maze test (*28*). During the learning period, the mice searched for the escape hole, and the latency time was recorded daily for 6 days. WT mice and MNPs-DP–treated PS19 mice learned a new task quicker with a shorter latency time to find the escape hole compared to the vehicle- or naked MNP-treated PS19 mice (Fig. 5B). After training, we examined their long-term memory by conducting a probe trial with the escape hole removed. Compared to the WT mice, the PBS- and MNP-treated PS19 model mice exhibited obvious memory deficits, including longer latency times (Fig. 5C), fewer target hole entries (Fig. 5D), and more random motion-like wandering paths (Fig. 5E). Also, PS19 mice treated with MNPs-DP displayed a comparable performance to WT mice and a significant improvement in memory function compared with PBS-treated PS19 mice, while MNPs did not show obvious improvement, indicating the specific activity of 7-DP (Fig. 5, C to E). These results suggest that 10 weeks of treatment with MNPs-DP tend to rescue spatial learning and memory deficits in the PS19 model mice of tauopathy.

In addition to the Barnes maze test, we used the novel object recognition test to evaluate the cognitive ability of mice (*29*). Briefly, the mice were first exposed to two identical objects for 10 min. After a 90-min interval, the mice were allowed to explore one of the familiar objects and a novel one. Cognitive ability can be evaluated by the difference between the exploration time of novel and familiar objects. We observed that WT mice and MNPs-DP–treated PS19 mice explored the novel object significantly longer than the familiar one, while unliganded MNP-treated PS19 mice did not show a difference in exploring the two objects and vehicle-treated PS19 mice spent more time exploring the familiar object (Fig. 5F). MNPs-DP treatment appeared to significantly improve the discriminatory index (DI; Fig. 5G) and discriminatory ratio (DR) (fig. S19) of the PS19 mice compared to vehicle-treated groups, while MNPs did not, indicating the specific activity of 7-DP.

## MNPs-DP do not cause obvious toxicity in PS19 mice

After the behavior tests, the mice were euthanized, and their blood, brains, and main organs were collected. It has been reported that MNPs are mainly cleared through the liver and spleen (*23*). Here, the aspartate aminotransferase (AST) blood test was used to assess the potential toxicity of MNPs-DP on liver function. The AST levels of MNPs-DP–treated mice were comparable to the vehicle groups, demonstrating that the long-term treatment of MNPs-DP under current dose did not lead to obvious liver damage (Fig. 5H). Histological analysis of the liver, spleen, heart, lung, and kidney (fig. S20) revealed no evidence of toxic changes

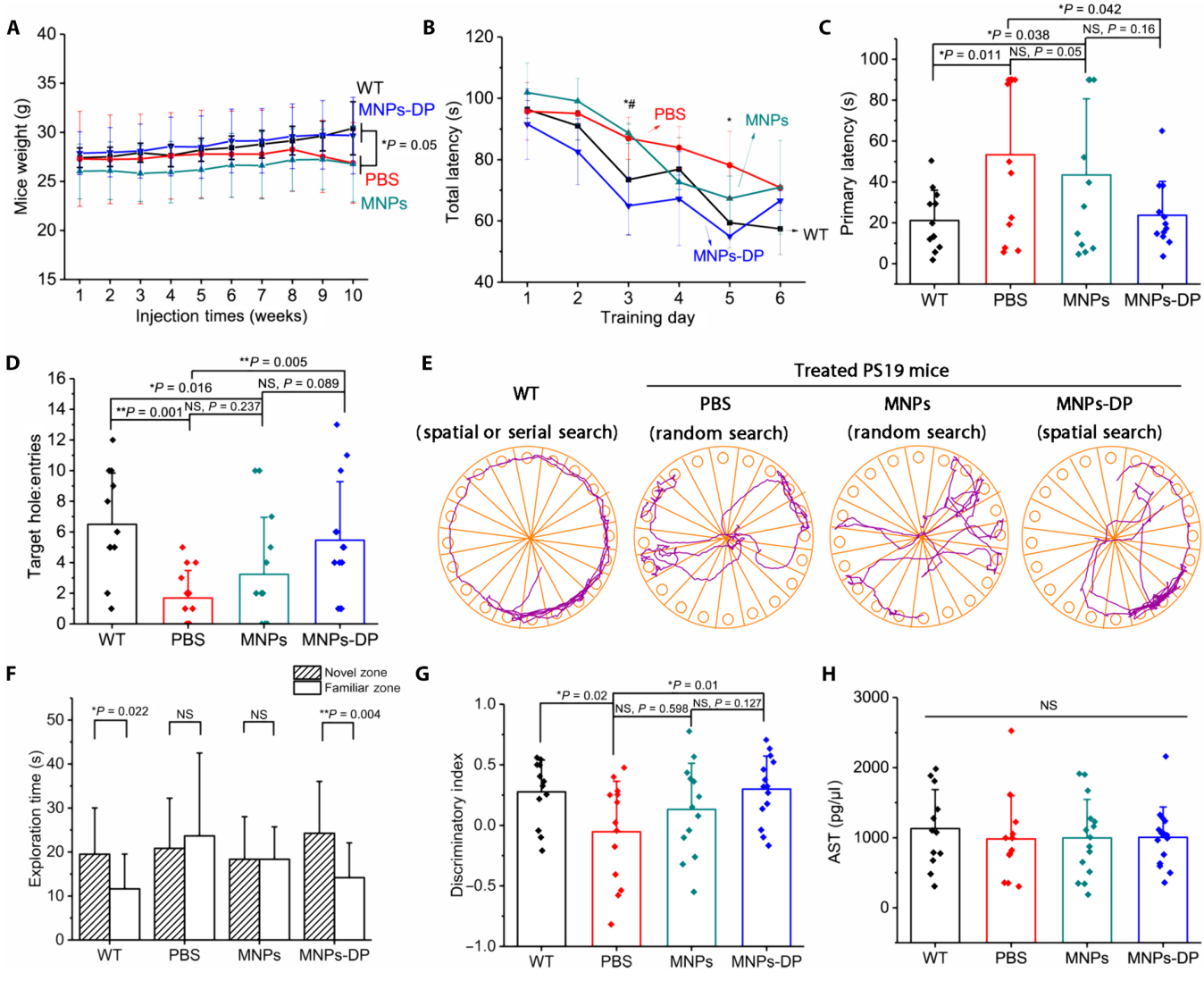


**Fig. 5. MNPs-DP rescues memory deficits in PS19 mice without causing obvious toxicity.** (**A**) Body weight of WT and PS19 mice treated with PBS, MNPs and MNPs-DP, respectively ($n = 13$ per group, eight male and five female mice for each group). (**B**) Total latency time to find the escape hole in the learning period for each group of mice ($n = 13$ per group, eight male and five female mice for each group). Statistical significance was analyzed by two-way ANOVA ($P < 0.05$; *MNPs-DP versus PBS; #MNPs-DP versus MNPs). (**C**) Primary latency for finding escape hole in the probe trial for each group of mice. (**D**) Entry number to target hole in probe test for each group of mice. (**E**) Representative track of probe test for each group of mice. (**F**) Time spent during the exploration of the familiar and novel objects in novel object recognition test ($n = 13$ per group, eight male and five female mice for each group). (**G**) Discriminatory index obtained in novel object recognition test. (**H**) Serum aspartate aminotransferase (AST) levels for each group of mice ($n = 13$ per group, eight male and five female mice for each group). Results shown as mean + SD ($n = 13$). Statistical significance was analyzed by two-way ANOVA (*$P < 0.05$; **$P < 0.01$).

or cell death in cellular structures between the MNPs-, MNPs-DP–, and vehicle-treated mice (*30*). In addition, the consistent increase in body weights of MNPs-DP–treated PS19 mice (blue line in Fig. 5A) also supported the biosafety of MNPs-DP with current dosing. Together, 10 weeks of treatment of MNPs-DP significantly rescue the spatial learning and memory impairments in a mouse model of AD without apparent toxic side effects in other body systems.

## MNPs-DP clear tau pathology in PS19 mice

To assess tau pathology of the mice, we immunostained brain sections with AT8, an antibody specific for phosphorylated tau (ptau) $pSer^{202}$/$Thr^{205}$ that is widely used to identify neurofibrillary tangles in postmortem human and PS19 mouse brains. WT mice did not show AT8-positive staining in the CA1 or CA3 regions, whereas a significant amount of AT8 positive ptau neurons with labeling resembling tau neurofibrillary tangles were found in the hippocampus of vehicle-treated PS19 mice ($n = 6$ per group; Fig. 6A and fig. S21). Impressively, MNPs-DP treatment significantly limited tau pathology in both the CA1 and CA3 regions, relative to the weak effect of unliganded MNPs (Fig. 6, A to C, and fig. S21). In addition, mouse brain tissues were analyzed for radioimmunoprecipitation assay (RIPA)–soluble and RIPA-insoluble tau by Western blot, with ptau levels normalized by β-actin levels (Fig. 6, D and E, and fig. S22). MNPs-DP significantly decreased both the insoluble and soluble ptau levels in the brain of PS19 mice ($n = 8$ per group; Fig. 6, F and G), consistent with the immunohistochemistry results.

## DISCUSSION

The development of tau-targeted therapeutics intended to slow the onset and progression of AD and other tauopathies remains an unfulfilled goal. Although numerous approaches have shown promise in animal models and preclinical studies, antitau therapeutics have yet to progress successfully beyond the early phases of clinical trials. Compounds with in vitro antitau amyloid activities have been identified; however, none have shown substantial success in placebo-controlled clinical trials. Their lack of in vivo efficacy could be due to factors such as limited bioavailability, poor metabolic stability, lack of specificity, and limited BBB permeability. New approaches are needed, and here and in other recent work (*11*, *12*), we suggest exploration of fragmentors of amyloid fibrils.

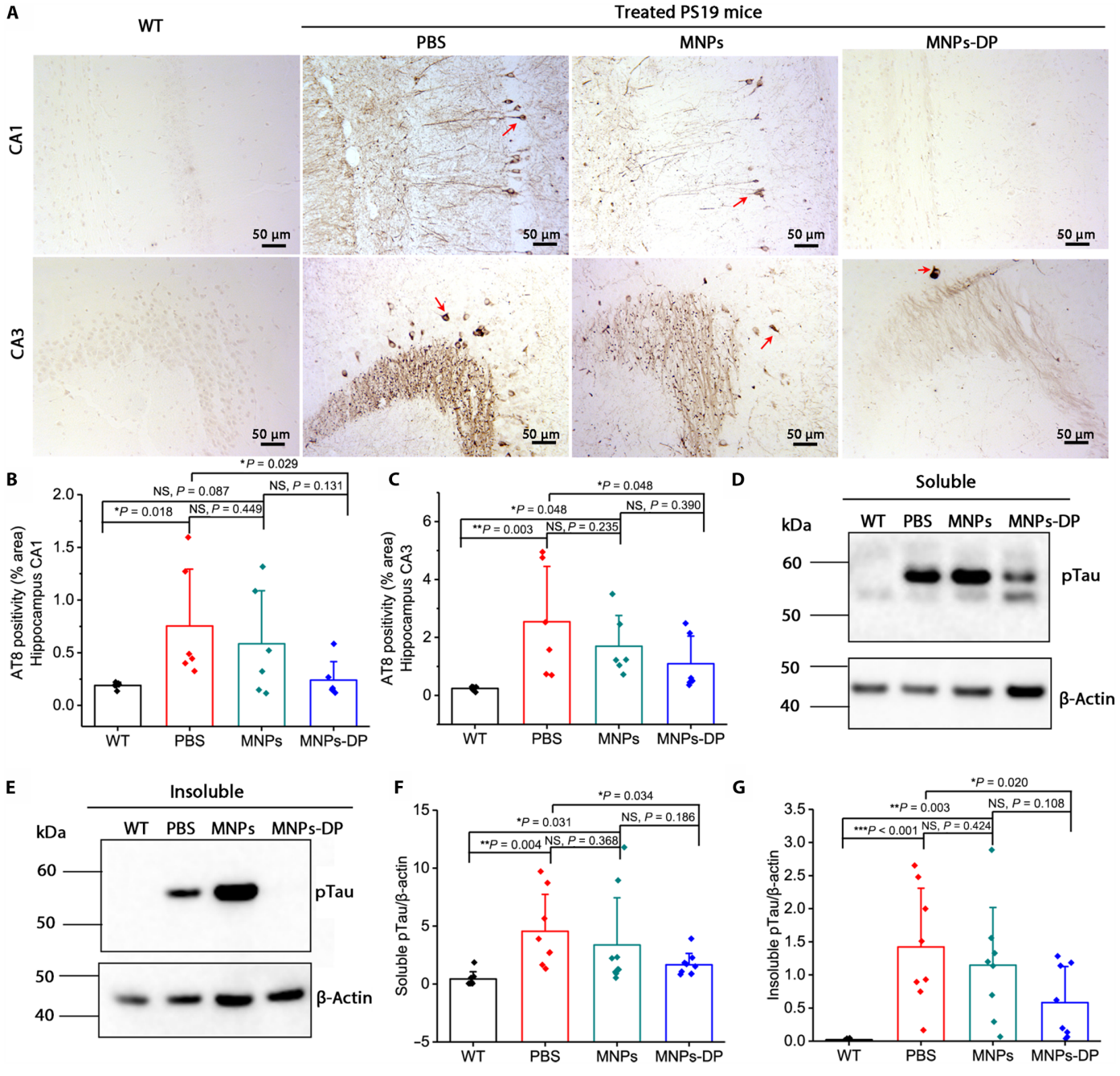


**Fig. 6. MNPs-DP reduce phosphorylated tau in the hippocampus of PS19 mice.** (**A**) Representative immunohistochemical images of the hippocampus (CA1 and CA3 regions) of WT and PS19 mice that treated with PBS, MNPs, and MNPs-DP, respectively, at ×10 magnification, stained with AT8 antibody for phosphorylated tau at residues $Ser^{202}/Thr^{205}$. The neurofibrillary tangles were indicated by red arrows. (**B**) Quantification of AT8-positive staining in the hippocampus CA1. (**C**) Quantification of AT8-positive staining in the hippocampus CA3. Representative Western blot for AT8 of (**D**) soluble and (**E**) insoluble hippocampus homogenates from WT and PS19 mice treated with PBS, MNPs, and MNPs-DP, respectively. β-Actin was used as a loading control. Quantification of (**F**) soluble phosphorylated tau (ptau) and (**G**) insoluble ptau normalized to β-actin ($n = 8$ per group, four male and four female PS19 mice for each group). Statistical significance was analyzed by two-way ANOVA (*$P < 0.05$; **$P < 0.01$; ***$P < 0.001$).

Here, we describe a nonnatural amino acid fragmentor of tau fibrils, D-TLKIVWC (7-DP), by modifying our previous structure-based inhibitor of tau fibrils, 6-DP (*10*). 7-DP not only inhibits the formation of tau aggregation but also fragments recombinant tau fibrils and tau fibrils isolated from the autopsied brains of patients with AD. Apparently, 7-DP can inhibit the prion-like spread of tau in biosensor cells and reduce tau-induced cellular toxicity in N2a cells by fragmentation. A potential concern about fragmenting amyloid fibrils is that the products of fragmentation could act as toxic oligomers, killing rather than protecting cells or acting as seeds that nucleate additional fibril formation (*31*). This is not the case for 7-DP as shown by the experiments described in Fig. 1.

Given the substantial stability of pathogenic amyloid, particularly of tau fibrils from AD postmortem brain (*32*), it is unexpected that a seven-residue peptide can fragment these fibrils readily at 37°C with no energy source other than of ambient thermal agitation and of mild shaking. While we have not yet fully determined the molecular mechanism of fragmentation, we have established some properties of 7-DP essential to its fragmenting ability. It must be at least seven residues in length; its six-residue analog D-TLKIVW does not fragment. Also, the sulfhydryl group of cysteine is not essential; it can be linked to MNP through a S—C bond without impairing fragmenting activity. The ability of 7-DP to form amyloid-like fibrils itself may be key, and we hypothesized a fragmentation mechanism as illustrated in Fig. 7.

We conjugated 7-DP to MNPs to facilitate its transport across the BBB. In addition, we intranasally injected 20 μl of 2% mannitol into mice to increase BBB permeability, but whether mannitol is necessary for effective uptake remains unknown and requires further testing. If it is found to be necessary, then coadministration of MNPs-DP and mannitol could be considered in a phase 1 trial through intravenous injection, similar to the US Food and Drug Administration–approved iron oxide nanoparticle drug Feraheme injection (*22*) (AMAG Pharmaceuticals) that contains mannitol. We believe that brain-deliverable peptides that fragment tau fibrils are promising precursors to possible future therapeutics of AD, but successful development will necessitate future studies of toxicity, pharmacokinetics, and distribution.

In summary, we provide preclinical data demonstrating the in vitro tau-fragmenting activity and the in vivo therapeutic potential of 7-DP and one intravenously bioavailable formulation on MNPs, MNPs-DP. Our work supports future phase 1 evaluation of 7-DP formulations including MNPs-DP in humans with AD and other tauopathies. If safe and acutely effective against tauopathy biomarkers, then this new class of highly specific structurally designed tau fragmentors could be optimized and further developed for clinical use.

## MATERIALS AND METHODS

### Recombinant tau protein expression and purification

Recombinant tau K18$^{+}$ (residues Gln$^{244}$ to Glu$^{380}$ of 4R tau) was expressed in a pNG2 vector in BL21-Gold *Escherichia coli* cells grown in LB to an $A_{600}$ = 0.8. Cells were induced with 0.5 mM isopropyl 1-thio-β-D-galactopyranoside for 3 hours at 37°C and lysed by sonication in 20 mM MES buffer (pH 6.8) with 1 mM EDTA, 1 mM

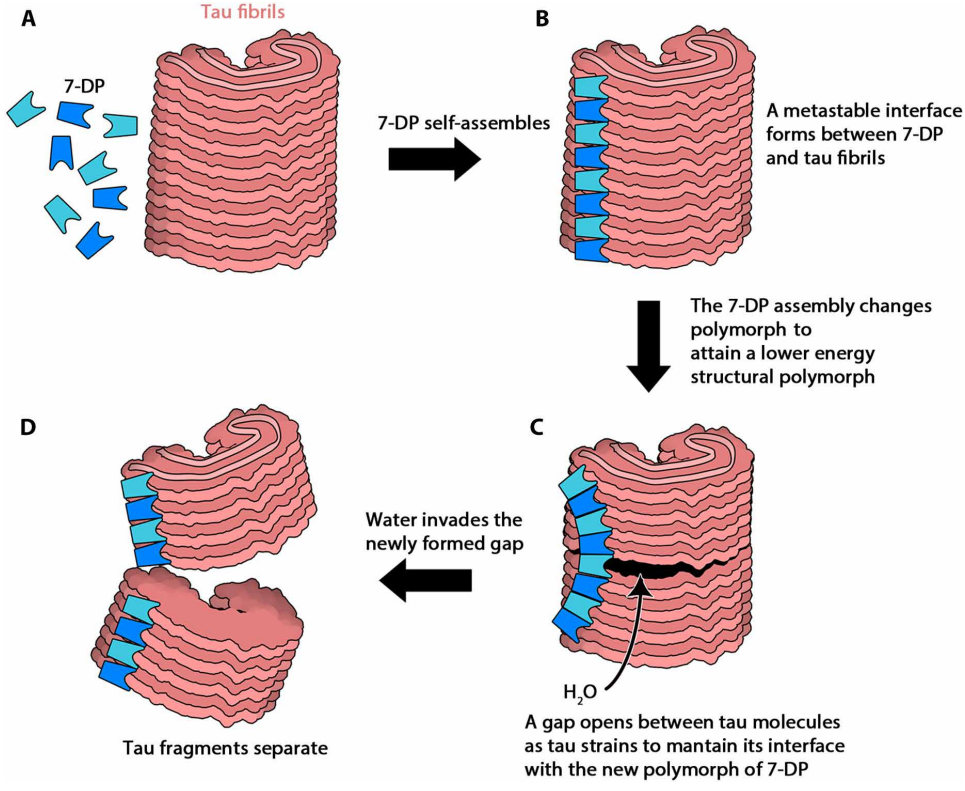


**Fig. 7. Hypothesized schematic mechanism of fragmentation of tau fibrils.** (**A**) Scheme illustrates the interaction of tau fibrils with 7-DP. (**B**) A metastable interface forms between 7-DP and tau fibrils because of self-assembly of 7-DP along tau fibrils. (**C**) A gap opens between tau molecules as the 7-DP assembly changes polymorph to attain a lower energy state and tau strains to maintain its interface with the new polymorph of 7-DP assembly. (**D**) Water invades the newly formed gap to fragment tau fragments.

$MgCl_2$, 1 mM dithiothreitol, and HALT protease inhibitor before the addition of NaCl (500 mM final concentration). Lysate was boiled for 20 min and then clarified by centrifugation at 15,000 rpm for 15 min and dialyzed to 20 mM MES buffer (pH 6.8) with 50 mM NaCl and 5 mM dithiothreitol. Dialyzed lysate was purified on a 5-ml HighTrap SP ion exchange column and eluted over a gradient of NaCl from 50 to 550 mM. Protein was further purified on a HiLoad 16/600 Superdex 75 pg column (GE Healthcare) in 10 mM tris (pH 7.6) with 100 mM NaCl and 1 mM dithiothreitol and concentrated to 20 to 60 mg/ml by ultrafiltration using a 3-kDa cut-off (Millipore-Sigma, Burlington, MA).

### Preparation of crude and purified AD brain tau fibrils

Tissue sections of 0.2 to 0.3 g were excised on a block of dry ice and manually homogenized in a 15-ml disposable tube in 1.5 ml of sucrose buffer with 1 mM EGTA and 5 mM EDTA. Samples were then aliquoted to polymerase chain reaction tubes and sonicated in a cuphorn bath for 120 min under 30% power at 4°C in a recirculating ice water bath to obtain the crude AD brain tau fibrils. For purification of tau fibrils from AD brain tissue, the crude AD brain tau samples were further heated at 90°C for 20 min in a thermal cycler and centrifuged at 20,100*g* for 30 min. The supernatant was collected and then spun at 90 K for 30 min on a Airfuge (Beckman-Coulter). Last, the pellet was the purified AD brain-derived tau fibrils and resuspended in 20 μl of 20 mM tris buffer with 100 mM NaCl and stored at 4°C.

### Synthesis of D-TLKIVWC liganded iron oxide nanoparticles MNPs-DP

Peptides were purchased from GenScript (Piscataway, NJ) and purified to ≥98%, as determined by mass spectrometry and high-performance liquid chromatography. The synthesis of D-TLKIVWC liganded iron oxide nanoparticles involves two steps. First, the carboxylic acid iron oxide MNPs (CD Bioparticles, WHM-G062) were reacted with 2-maleimidoethylamine hydrochloride to gain the maleimide-functionalized iron oxide nanoparticles, which were further conjugated with D-TLKIVWC to obtain the MNPs-D-TLKIVWC through the thiol-maleimide Michael addition click reaction. Briefly, 1 mg of *N*-hydroxysulfosuccinimide (Thermo Fisher Scientific) and 1.5 mg of *N*-ethyl-*N*′-(3-(dimethylamino)propyl) carbodiimide (Thermo Fisher Scientific) were dissolved in 50 μl activation buffer [0.1 M MES and 0.5 M NaCl (pH 6.0)] separately before they were added to the 200 μl MNPs (5 mg/ml) with 100 μl of activation buffer and kept shaken at room temperature for 15 min. Next, 2 mg of 2-maleimidoethylamine hydrochloride that dissolved in 500 μl of 20× PBS was added to the above solution and kept shaken at room temperature for another 2 hours. After that, the solution was kept in a magnetic separator in 4°C. After three times of magnetic separation and washing, the supernatant was removed, and the nanoparticles were resuspended in 1 ml of 1× tris buffer (pH 7.04) by sonication for several hours. In the second step, 4 mg of D-TLKIVWC was dissolved in 1× tris buffer (pH 7.04) and then added to the above MNP solution. The mixed solution was kept rotated at room temperature for 1 hour before left in a magnetic separator. All samples were washed with deionized water for three times to remove the surface-adsorbed 7-DP. The supernatant in all washing process was combined with the supernatant in the magnetic separator process. Then, the absorbance intensity of the combined supernatant at 280 nm was measured using the NanoDrop One (Thermo Fisher Scientific). The conjugation efficacy (%) of 7-DP on MNPs can be calculated following $(M_i - M_S)/M_S$, where $M_i$ is the initial amount of 7-DP used, and $M_S$ is the amount of 7-DP in the supernatant. The morphology of the nanoparticles was observed by FEI Tecnai T12 Quick room temperature TEM at 120 kV. The zeta potential and hydrodynamic diameters of the nanoparticles were measured using a ZetaSizer Nano ZS90 (Malvern Instruments).

### ThT inhibition assay

Frozen aliquot of the purified recombinant tau $K18^+$ was thawed on ice and diluted into PBS (pH 7.4) to a final concentration of 20 μM. In vitro aggregation was initiated by incubating 150 μl, 20 μM tau $K18^+$ monomer in the presence of 40 μM ThT, 15 μM heparin (H3393, Sigma-Aldrich), and 1 mM dithiothreitol in a black Nunc 96-well optical bottom plate (Thermo Fisher Scientific). To test the effect of D-TLKIVWC, D-TLKIVW, MNPs-DP, MNPs, and MNPs-DPsc on inhibiting tau $K18^+$ aggregation, tau $K18^+$ monomer was incubated in the presence of different concentrations of D-TLKIVW/D-TLKIVWC (5, 10, 20, 50, and 100 μM), MNPs-DP/MNPs/MNPs-DPsc (0.005, 0.01, 0.02, and 0.04 mg/ml) in parallel. Kinetic fluorescence data were collected in a microplate reader (FLUOstar Omega, BMG Labtech) at 37°C with double orbital shaking at 700 rpm. Fluorescence measurements were recorded every 10 min with excitation and emission wavelengths of 440 and 480 nm. All samples were added in triplicate, and experiments were repeated at least three runs.

### ThT fragmentation assay

Tau $K18^+$ monomer (20 μM) was grown in the presence of 40 μM ThT, 15 μM heparin, and 1 mM dithiothreitol overnight to form the fibrils. The tested D-TLKIVWC, D-TLKIVW, MNPs-DP, or MNPs were added separately in parallel to designated wells, and the ThT assay was further continued. Kinetic fluorescence data were collected in a microplate reader (FLUOstar Omega, BMG Labtech) at 37°C with double orbital shaking at 700 rpm. Fluorescence measurements were recorded every 10 min with excitation and emission wavelengths of 440 and 480 nm. All samples were added in triplicate, and experiments were repeated at least twice. After 24 hours of incubation, the samples were collected for TEM and dot blot studies.

### Transmission electron microscopy

Six microliters of sample was applied to a glow discharged carbon coated electron microscopy grid (CF150-Cu, Electron Microscopy Sciences) for 5 min. Then, grids were stained with 2% uranyl acetate for 2 min. Samples were visualized using a FEI Tecnai T12 Quick room temperature transmission electron microscope using an acceleration voltage of 120 kV equipped with a Gatan 2048 × 2048 charge-coupled device camera.

### Circular dichroism

The measurements were conducted on Chirascan Q100 CD spectrometer (Applied Photophysics Limited, UK). Samples were measured in a quartz cell (0.5 mm), and the wavelength was set in the range between 190 and 250 nm. Accumulation was conducted three times continuously for each sample.

### Native electrospray–ionization mass spectrometry

Samples were buffer-exchanged into 20 mM ammonium acetate with 0.5 ml of 10 kDa Amicon filters (Millipore-Sigma, Burlington,

MA). The samples were then measured using a Synapt G2-Si (Waters Corporation Milford, MA). All protein solutions were loaded into in-house pulled capillaries coated with gold and electrosprayed by applying a capillary voltage between 1 and 2 kV on the nanoelectrospray ionization source. The native electrospray–ionization mass spectrometry experiment was repeated twice to demonstrate reproducibility.

### Fragmentation of purified AD brain-derived tau fibrils

Purified AD brain tau fibrils were incubated with D-TLKIVWC (25, 50, 100, 250, and 500 μM) and D-TLKIVW (500 μM) at 37°C for 48 hours, respectively. The samples were collected for TEM characterization, dot blot, and Western blot studies. The TEM protocol was the same as above. The number of AD tau fibrils in each image was counted ($n$ = 10 images). For dot blot study, 2.5 μl of samples was added on nitrocellulose membrane (0.2 μm, Bio-Rad). The membrane was blocked by 5% (w/v) nonfat dry milk in TBS-T [T = 0.1% (v/v) Tween-20] at room temperature for 1 hour. After blocking, the membrane was incubated with GT38 antibody obtained from Virginia Lee's lab (1:1000) in 5% (w/v) milk in TBS-T at 4°C overnight. Then, the membrane was washed in TBS-T for three times and incubated with goat anti-mouse immunoglobulin G horseradish peroxidase (HRP; 1:5000; catalog no. AB205719, Abcam) in TBS-T for 1 hour at room temperature. The membrane was washed three more times, and the signal was developed with Pierce ECL Western blotting substrate (170-5061, Bio-Rad). The samples were centrifuged at 21,000*g* for 30 min at 4°C (Eppendorf Centrifuge 5424R). Western blot was performed with antitau rabbit polyclonal antibody (1:1000; Dako, A0024) and anti-rabbit HRP-conjugated secondary antibody (1:5000; Thermo Fisher Scientific).

### Fragmentation of tau aggregates in HEK293 cells

HEK293 cell lines were purchased from the American Type Culture Collection (CRL-1573). Cells were maintained in Dulbecco's modified Eagle's medium (Life Technologies, catalog no. 11965092) supplemented with 10% (v/v) fetal bovine serum (Life Technologies, catalog no. A3160401), 1% penicillin/streptomycin (Life Technologies, catalog no. 15140122), and 1% GlutaMAX (Life Technologies, catalog no. 35050061) at 37°C, 5% $CO_2$ in a humidified incubator. pcDNA3.1 for 1N4R tau with a P301S mutation was a gift from M. Goedert at the Medical Research Council Laboratory of Molecular Biology in Cambridge, UK. Crude AD brain tau fibrils were sonicated for 1 min before they were transfected to cells together with tau pcDNA3.1. After 24 hours. 7-DP at various concentrations with or without 10 μM MG132 (Thermo Fisher Scientific) were transfected into cells using Lipofectamine 2000 (Life Technologies, catalog no. 11668019). After another 24-hour incubation, cells were collected using 100 μl of lysing buffer [10 mM tris (pH 7.4), 200 mM NaCl, 1 mM EDTA, 0.5% deoxycholate, and 0.5% Triton X-100] and sonicated in a cuphorn water bath for 10 min. The lysed cells were ultracentrifuged at 90,000 rpm in a Beckman Coulter Airfuge Air-driven Ultracentrifuge. The supernatant was collected and labeled "supernatant," and the pellet was resuspended in 100 μl of PBS and labeled "pellet." An equalized amount of each sample was run on a NuPAGE 4 to 12%, bis-tris, 1.0 mm, Mini Protein Gel (15-well). Western blot was performed with antitau rabbit polyclonal antibody (1:1000; Dako, A0024) and anti-rabbit HRP-conjugated secondary antibody (1:5000; Thermo Fisher Scientific). β-Actin was used as a loading control (1:2000; sc-47778, Santa Cruz Biotechnology).

### Fragmentation of tau aggregates in tau biosensor cell line

HEK293 cell lines stably expressing EYFP-fused tau 1N4R P301S were engineered by M. Diamond's laboratory at the University of Texas Southwestern Medical Center and used without further characterization or authentication. Crude AD brain tau fibrils were sonicated for 1 min before they were transfected to cells. After 24 hours, 7-DP or PBS was transfected into cells using Lipofectamine 2000 (Life Technologies, catalog no. 11668019). After another 24-hour incubation, the number of seeded aggregates was determined by imaging the entire well of a 96-well plate in triplicate using a Celigo image cytometer (Nexcelom) in the YFP channel. Aggregates were counted using ImageJ by subtracting the background fluorescence from unseeded cells and then counting the number of peaks with fluorescence above background using the built-in particle analyzer. The number of aggregates was normalized to the confluence of each well, and dose-response plots were generated by calculating the average and SD values from triplicate measurements. For high-quality images, cells were photographed on a ZEISS Axio Observer D1 fluorescence microscope using the YFP fluorescence channel.

### Crude AD brain tau fibril seeding in tau biosensor cell line

HEK293 cell lines stably expressing tau-K18-YFP were engineered by M. Diamond's laboratory at the University of Texas Southwestern Medical Center and used without further characterization or authentication. Cells were maintained in Dulbecco's modified Eagle's medium supplemented with 10% (v/v) fetal bovine serum, 1% antibiotic-antimycotic, and 1% GlutaMAX at 37°C, 5% $CO_2$ in a humidified incubator. Crude AD brain tau fibrils were incubated with D-TLKIVWC (5, 10, 20, 50, 75, and 100 μM), D-TLKIVW (5, 10, 20, 50, 75, and 100 μM), MNPs-DP (0.005, 0.01, 0.02, and 0.04 mg/ml), or MNPs (0.005, 0.01, 0.02, and 0.04 mg/ml) overnight and sonicated in a cup horn water bath for 3 min. Then, these inhibitor/fragmentor-treated tau seeds were mixed with 1 volume of Lipofectamine 3000 prepared by diluting 1 μl of Lipofectamine in 19 μl of OptiMEM. After 20 min, 10 μl of fibrils was added to 90 μl of tau biosensor cells. In some cases, the D-TLKIVWC and AD tau seeds were directly transfected to the cells without incubation overnight. After 24 hours of incubation, the number of seeded aggregates was determined by imaging the entire well of a 96-well plate in triplicate using a Celigo image cytometer (Nexcelom) in the YFP channel. The data analysis was described before. For high-quality images, cells were photographed on a ZEISS Axio Observer D1 fluorescence microscope using the YFP fluorescence channel.

### Cell viability of tau K18$^+$ aggregates

Tau K18$^+$ aggregates were produced by incubation of tau K18$^+$ (20 μM) in the absence or presence of D-TLKIVWC (5, 10, 20, 50, and 100 μM), D-TLKIVW (5, 10, 20, 50, and 100 μM), MNPs-DP (0.005, 0.01, 0.02, and 0.04 mg/ml), or MNPs (0.005, 0.01, 0.02, and 0.04 mg/ml) for 48 hours in PBS, respectively. PBS without any protein was used as controls. N2a cells were cultured in minimum essential medium supplemented with 10% (v/v) fetal bovine serum, 1% antibiotic-antimycotic, and 1% GlutaMAX in a 5% $CO_2$ humidified environment at 37°C. Cells were plated at a density of 10,000 cells per well on 96-well plates in 90 μl of fresh medium. After 24 hours, 10 μl of the above tau K18$^+$ aggregates was added, and the cells were incubated for another 24 hours at 37°C. Cytotoxicity was measured using the MTT assay. Ten microliters of the stock MTT reagent (5 mg/ml) was added to each well.

After 3 hours of conversion into the formazan product, dimethyl sulfoxide (DMSO; Thermo Fisher Scientific) was added to dissolve the purple crystals left in the dark for 10 min before the measurement of absorbance at 570 nm with 700 nm as a subtracted reference wavelength using a microplate reader (SpectraMax M5, Molecular Devices, USA). Cells treated with 100% DMSO were designated as 0% viable, and those treated only with vehicle were designated as 100% viable. To further investigate the cytotoxicity of compounds alone, various concentrations of D-TLKIVWC (final concentration in wells is 2, 5, 10, 20, 50, 100, or 200 μM), D-TLKIVW (final concentration in wells is 2, 5, 10, 20, 50, 100, or 200 μM), MNPs (final concentration in wells is 0.0025, 0.005, 0.01, 0.02, or 0.04 mg/ml), or MNPs-DP (final concentration in wells is 0.0025, 0.005, 0.01, 0.02, or 0.04 mg/ml) were dispensed into the N2a cells and further incubated for 24 hours at 37°C and in 5% $CO_2$ incubator. Cytotoxicity was measured using a MTT assay.

### Cell toxicity of tau K18$^+$ fibril fragmentation species

Tau K18$^+$ fibril fragmentation species were produced by incubating tau K18$^+$ fibrils with D-TLKIVWC (5, 10, 20, 50, or 100 μM), D-TLKIVW (5, 10, 20, 50, or 100 μM), MNPs-DP (0.005, 0.01, 0.02, or 0.04 mg/ml), or MNPs (0.005, 0.01, 0.02, or 0.04 mg/ml) for 24 hours, respectively. N2a cells were cultured in MEM supplemented with 10% (v/v) fetal bovine serum, 1% antibiotic-antimycotic, and 1% GlutaMAX in a 5% $CO_2$ humidified environment at 37°C. Cells were plated at a density of 10,000 cells per well on 96-well plates in 90 μl of fresh medium. After 24 hours, 10 μl of the above tau K18$^+$ fibril fragmentation species was added, and the cells were incubated for another 24 hours at 37°C. Cytotoxicity was measured using MTT assay as above.

### Animals

P301S transgenic mice (Prnp-MAPT*P301S PS19Vle/J, JAX stock #008169, the Jackson Laboratory, Bar Harbor, ME) and C57BL/6J mice (the Jackson Laboratory, JAX:000664) were housed in groups of up to four in individually ventilated cages under standard conditions (22°C, 12-hour light-dark cycle) receiving food and water ad libitum. All animal experiments were performed in accordance with the National Institutes of Health regulations and approved by UCLA Animal Research Committee and performed under oversight of the Division of Laboratory Animal Medicine.

### Inductively coupled plasma mass spectrometry

The iron contents of brain tissues were assessed by ICP-MS (NexION 2000, PerkinElmer). The half brain tissues were dried at 105°C to constant weight; 1 ml of concentrated nitric acid and 0.2 ml of concentrated hydrochloric acid were added to the weighted sample (100 mg) in a tube and heated at 80°C for 2 hours. After digestion, the solution was diluted to 10 ml with deionized water for ICP-MS tests.

### Treatments

We stereotaxically seeded 24 2-month-old, male PS19 mice and 15 6-month-old, female PS19 mice with 1.5 μl of recombinant K18$^+$ tau fibril seeds (5 μg/μl) and divided those 39 mice into three groups ($n = 13$ per group, eight male and five female mice for each group). Each group was intravenously administered with vehicle, unliganded MNPs, or MNPs-DP (10 mg/kg of body weight) every week for 10 weeks. The weight of mice was recorded weekly. Treatment with unliganded MNPs or MNPs-DP was always in combination with intranasal administration of mannitol. WT, age-matched C57BL/6 mice were stereotaxically injected with vehicle to serve as controls.

### Behavioral tests

All behavioral experiments were conducted in the Behavioral Testing Core (BTC) at UCLA. Mice were transferred to the BTC and allowed to acclimate for 1 week. All the animals were handled for at least three to four consecutive days before testing. They were tested in random order, and the experimenter conducting the tests was unaware of the genotype/group.

### Barnes maze

The maze consisted of a circular platform with 20 holes around the periphery with an escape box attached to the bottom of one of the holes and shallow boxes attached to the bottom of the other holes. Bright light and white noise were used to motivate mice to find and enter the escape box. Visual extra-maze cues were present on three walls of the room. For all trials, mice were placed individually in a cylindrical start chamber in the center of the maze for 30 s, which was then lifted to start the test. During an adaptation period, mice were guided to the escape tunnel and allowed to stay there for 30 s. During a spatial acquisition period, a total of 10 acquisition trials (two trials per day with an intertrial interval of 15 min) were performed; mice were allowed to explore the maze freely for 2 min. Each trial ended when the mouse entered the escape tunnel or after 2 min had elapsed. Mice that did not find the tunnel were guided to it. All mice were allowed to remain in the tunnel for 30 s. During the probe trial conducted 1 day after the last training trial, the escape tunnel was replaced by a shallow box, and mice were allowed to explore the maze for 90 s. Animals' performances were monitored using Any-Maze Video Tracking System (Stoelting Co., Wood Dale, IL), which provided data for the acquisition parameter (latency to find the platform) and the probe trial parameters (latency to find the platform, number of entries in the target platform zone of the platform).

### Novel object recognition

Mice were habituated to the open testing arena for 10 min, 24 hours before the test was performed. During the memory acquisition trial, each mouse was allowed to explore two identical objects for 10 min. The mice were returned to their home cage for 90 min. For the memory retention phase, animals were exposed for 10 min to the presence of one similar object and one novel object (a different shape and color). Object exploration time was recorded when the mouse touched the object directly with its nose, mouth, or forepaws. Results are expressed as exploration time for each object. The cognitive function was evaluated by the DR and DI, which is represented by TC/(TR + TC) and (TR − TC)/(TR + TC), respectively, where TC is the time spent exploring the novel object, and TR is the time spent exploring the familiar object.

### Determination of blood AST levels as an index of hepatic toxicity

Blood samples were obtained by cardiac puncture and centrifuged at 2000*g* for 20 min to separate the serum for collection. Activities AST was assayed using Mouse AST enzyme-linked immunosorbent assay kits (Abcam, ab263882) according to the manufacturer's protocols.

### Hematoxylin and eosin staining

Major organs including heart, liver, spleen, lung, and kidney ($n = 3$) were fixed in 4% buffered formalin saline (Sigma-Aldrich) at 4°C overnight and then embedded in paraffin blocks. Tissue sections of 5 μm thickness were stained with hematoxylin and eosin (H&E). The morphology of the tissue was observed under a light microscope (Leica) at ×20 magnification.

### Immunohistochemistry

The brain tissues were embedded in paraffin and sectioned at 10-μm thickness. Following deparaffinization, rehydration, heat-induced antigen retrieval in citrate buffer (pH 6.0), and blocking of endogenous peroxidase activity by 3% hydrogen peroxide, the sections were incubated with the antitau (1:500; AT8, monoclonal, mouse, Innogenetics) at 4°C overnight. On the second day, followed by being washed three times in TBST, 5 min each, the sections were incubated in biotinylated anti-mouse secondary antibody (1:1000) in 1.5% normal serum with 3% bovine serum albumin/tris-buffered saline for 1 hour at 37°C. Immunolabeling was detected using the avidin-biotinylated HRP complex method (Elite Kit, Vector, USA) and was visualized with diaminobenzidine (Wako, Japan). Last, the sections were mounted onto coverslips using DPX mounting media (Thermo Fisher Scientific). The images were collected at ×10 magnification with a digital MC170 5 MPixel Leica camera on a Nikon Eclipse E800M microscope. Image processing and analysis were performed with the ImageJ software. Macros were developed for each staining to attain a reproducible semi-automated quantification. The image files were converted to eight-bit grayscale. A uniform threshold value of 50 (using the dark background option) was then applied before performing the "analyze particles" task to determine the percent of area covered by positive signal.

### Western blot analyses

PBS-perfused unfixed brains were used for biochemical analysis by dissecting the hippocampi separately. Before analysis, the brain samples were sonicated in RIPA buffer (4 vol/g) [50 mM tris, 150 nM NaCl, 0.1% SDS, 0.5% sodium deoxycholate, 1% NP-40, 5 mM EDTA, 1 mM phenylmethylsulfonyl fluoride, 0.1% protease inhibitor mixture, and 0.5% phosphatase inhibitor (pH 8.0)] and centrifuged at 100,000*g* for 30 min at 4°C. The supernatants were saved as RIPA-soluble fractions, whereas the RIPA-insoluble pellets were washed with 1 M sucrose in RIPA buffer to remove myelin and associated lipids and centrifuged at 100,000g for 30 min at 4°C. The RIPA-insoluble pellets were then extracted in tissue (1 vol/g) with 2% SDS buffer [50 mM tris-HCl (pH 7.6)]. The protein contents of the samples were measured using the BCA Protein Assay Kit (Pierce, Bonn, Germany) and diluted to the same concentration (500 μg/ml). Soluble and insoluble fractions were analyzed by SDS-PAGE, followed by Western blotting using AT8 antibody (1:200; MN1020, Thermo Fisher Scientific). β-Actin was used as a loading control (1:2000; sc-47778, Santa Cruz Biotechnology). Bands were quantified using ImageJ software.

### Statistical analysis

Graphs are expressed as means + SD, and data were analyzed using SPSS 19.0 statistical analysis software (SPSS, Chicago, IL, USA). Two-way analysis of variance (ANOVA) followed by a least significant difference posttest were used to analyze difference among multiple groups. Statistical differences for all tests were considered significant at the $^{*}P < 0.05$, $^{**}P < 0.01$, and $^{***}P < 0.001$ levels; NS, not significant.

## Supplementary Materials

**This PDF file includes:**

Figs. S1 to S22

## REFERENCES AND NOTES


1. H. Braak, E. Braak, Neuropathological stageing of Alzheimer-related changes. *Acta Neuropathol.* **82**, 239–259 (1991).
2. P. V. Arriagada, J. H. Growdon, E. T. Hedley-Whyte, B. T. Hyman, Neurofibrillary tangles but not senile plaques parallel duration and severity of Alzheimer's disease. *Neurology* **42**, 631–639 (1992).
3. S. Asher, R. Priefer, Alzheimer's disease failed clinical trials. *Life Sci.* **306**, 120861 (2022).
4. L. VandeVrede, A. L. Boxer, M. Polydoro, Targeting tau: Clinical trials and novel therapeutic approaches. *Neurosci. Lett.* **731**, 134919 (2020).
5. A. Mullard, Anti-tau antibody failures stack up. *Nat. Rev. Drug Discov.* **20**, 888 (2021).
6. J. M. Ringman, S. A. Frautschy, E. Teng, A. N. Begum, J. Bardens, M. Beigi, K. H. Gylys, V. Badmaev, D. D. Heath, L. G. Apostolova, V. Porter, Z. Vanek, G. A. Marshall, G. Hellemann, C. Sugar, D. L. Masterman, T. J. Montine, J. L. Cummings, G. M. Cole, Oral curcumin for Alzheimer's disease: Tolerability and efficacy in a 24-week randomized, double blind, placebo-controlled study. *Alzheimers Res. Ther.* **4**, 43 (2012).
7. C. M. Wischik, C. R. Harrington, J. M. Storey, Tau-aggregation inhibitor therapy for Alzheimer's disease. *Biochem. Pharmacol.* **88**, 529–539 (2014).
8. M. Faiyaz, M. A. Ganayee, S. Akhtar, S. Krishnan, B. Flora, D. Dogra, N. K. Jha, D. K. Chellappan, P. Negi, K. Dua, Nanomaterials in Alzheimer's disease treatment: A comprehensive review. *Front. Biosci.* **26**, 851–865 (2021).
9. S. Luo, C. Ma, M. Q. Zhu, W. N. Ju, Y. Yang, X. Wang, Application of iron oxide nanoparticles in the diagnosis and treatment of neurodegenerative diseases with emphasis on Alzheimer's disease. *Front. Cell. Neurosci.* **14**, 21 (2020).
10. S. A. Sievers, J. Karanicolas, H. W. Chang, A. Zhao, L. Jiang, O. Zirafi, J. T. Stevens, J. Münch, D. Baker, D. Eisenberg, Structure-based design of non-natural amino-acid inhibitors of amyloid fibril formation. *Nature* **475**, 96–100 (2011).
11. P. M. Seidler, K. A. Murray, D. R. Boyer, P. Ge, M. R. Sawaya, C. J. Hu, X. Cheng, R. Abskharon, H. Pan, M. A. DeTure, C. K. Williams, D. W. Dickson, H. V. Vinters, D. S. Eisenberg, Structure-based discovery of small molecules that disaggregate Alzheimer's disease tissue derived tau fibrils in vitro. *Nat. Commun.* **13**, 5451 (2022).
12. K. A. Murray, C. J. Hu, H. Pan, J. Lu, R. Abskharon, J. T. Bowler, G. M. Rosenberg, C. K. Williams, G. Elezi, M. Balbirnie, K. F. Faull, H. V. Vinters, P. M. Seidler, D. S. Eisenberg, Small molecules disaggregate alpha-synuclein and prevent seeding from patient brain-derived fibrils. *Proc. Natl. Acad. Sci. U.S.A.* **120**, e2217835120 (2023).
13. P. Chong, C. Sia, B. Tripet, O. James, M. Klein, Comparative immunological properties of enantiomeric peptides. *Lett. Pept. Sci.* **3**, 99–106 (1996).
14. P. M. Seidler, D. R. Boyer, K. A. Murray, T. X. P. Yang, M. Bentzel, M. R. Sawaya, G. Rosenberg, D. Cascio, C. K. Williams, K. L. Newell, B. Ghetti, M. A. DeTure, D. W. Dickson, H. V. Vinters, D. S. Eisenberg, Structure-based inhibitors halt prion-like seeding by Alzheimer's disease–and tauopathy–derived brain tissue samples. *J. Biol. Chem.* **294**, 16451–16464 (2019).
15. O. A. Morozova, Z. M. March, A. S. Robinson, D. W. Colby, Conformational features of tau fibrils from Alzheimer's disease brain are faithfully propagated by unmodified recombinant protein. *Biochemistry* **52**, 6960–6967 (2013).
16. W. Zhang, B. Falcon, A. G. Murzin, J. Fan, R. A. Crowther, M. Goedert, S. H. W. Scheres, Heparin-induced tau filaments are polymorphic and differ from those in Alzheimer's and Pick's diseases. *eLife* **8**, e43584 (2019).
17. A. W. P. Fitzpatrick, B. Falcon, S. He, A. G. Murzin, G. Murshudov, H. J. Garringer, R. A. Crowther, B. Ghetti, M. Goedert, S. H. W. Scheres, Cryo-EM structures of tau filaments from Alzheimer's disease. *Nature* **547**, 185–190 (2017).
18. T. Hamano, T. F. Gendron, L. W. Ko, S. H. Yen, Concentration-dependent effects of proteasomal inhibition on tau processing in a cellular model of tauopathy. *Int. J. Clin. Exp. Pathol.* **2**, 561–573 (2009).
19. S. B. Prusiner, A unifying role for prions in neurodegenerative diseases. *Science* **336**, 1511–1513 (2012).
20. M. Goedert, Alzheimer's and Parkinson's diseases: The prion concept in relation to assembled Aβ, tau, and α-synuclein. *Science* **349**, 1255555 (2015).
21. B. B. Holmes, J. L. Furman, T. E. Mahan, T. R. Yamasaki, H. Mirbaha, W. C. Eades, L. Belaygorod, N. J. Cairns, D. M. Holtzman, M. I. Diamond, Proteopathic tau seeding predicts tauopathy in vivo. *Proc. Natl. Acad. Sci.* **111**, E4376–E4385 (2014).

22. M. Lu, M. H. Cohen, D. Rieves, R. Pazdur, FDA report: Ferumoxytol for intravenous iron therapy in adult patients with chronic kidney disease. *Am. J. Hematol.* **85**, 315–319 (2010).
23. H. Arami, A. Khandhar, D. Liggitt, K. M. Krishnan, In vivo delivery, pharmacokinetics, biodistribution and toxicity of iron oxide nanoparticles. *Chem. Soc. Rev.* **44**, 8576–8607 (2015).
24. S. Belbekhouche, M. Guerrouache, B. Carbonnier, Thiol-maleimide michael addition click reaction: A new route to surface modification of porous polymeric monolith. *Macromol. Chem. Phys.* **217**, 997–1006 (2016).
25. A. M. Jackson, J. W. Myerson, F. Stellacci, Spontaneous assembly of subnanometre-ordered domains in the ligand shell of monolayer-protected nanoparticles. *Nat. Mater.* **3**, 330–336 (2004).
26. M. Schweighauser, A. G. Murzin, J. Macdonald, I. Lavenir, R. A. Crowther, H. S. Scheres, M. Goedert, Cryo-EM structures of tau filaments from the brains of mice transgenic for human mutant P301S Tau. *Acta Neuropathol. Commun.* **11**, 160 (2023).
27. M. Iba, J. L. Guo, J. D. McBride, B. Zhang, J. Q. Trojanowski, V. M. Lee, Synthetic tau fibrils mediate transmission of neurofibrillary tangles in a transgenic mouse model of Alzheimer's-like tauopathy. *J. Neurosci.* **33**, 1024–1037 (2013).
28. K. Gawel, E. Gibula, M. Marszalek-Grabska, J. Filarowska, J. H. Kotlinska, Assessment of spatial learning and memory in the Barnes maze task in rodents-methodological consideration. *Naunyn Schmiedebergs Arch. Pharmacol.* **392**, 1–18 (2019).
29. M. Leger, A. Quiedeville, V. Bouet, B. Haelewyn, M. Boulouard, P. Schumann-Bard, T. Freret, Object recognition test in mice. *Nat. Protoc.* **8**, 2531–2537 (2013).
30. T. K. Jain, M. K. Reddy, M. A. Morales, D. L. Leslie-Pelecky, V. Labhasetwar, Biodistribution, clearance, and biocompatibility of iron oxide magnetic nanoparticles in rats. *Mol. Pharm.* **5**, 316–327 (2008).
31. E. Nachman, A. S. Wentink, K. Madiona, L. Bousset, T. Katsinelos, K. Allinson, H. Kampinga, W. A. McEwan, T. R. Jahn, R. Melki, Disassembly of Tau fibrils by the human Hsp70 disaggregation machinery generates small seeding-competent species. *J. Biol. Chem.* **295**, 9676–9690 (2020).
32. M. R. Sawaya, M. P. Hughes, J. A. Rodriguez, R. Riek, D. S. Eisenberg, The expanding amyloid family: Structure, stability, function, and pathogenesis. *Cell* **184**, 4857–4873 (2021).

**Acknowledgments:** We thank the organ donors and their families; without whom this work would not have been possible. The authors thank M. Diamond for sharing the YFP-labeled tau K18 expressing HEK293 cells. The behavior tests were conducted in the BTC facility under the supervision of L. M. Lueptow and I. Zhuravka. We acknowledge UCLA Tissue Pathology Core Laboratory (TPCL) for H&E staining. We thank C. H. Chang at the ICP-MS facility of UCLA for analysis of the Fe concentration in brain tissues. We acknowledge Y. Jiang for discussion, M. Goedert for the pcDNA3.1 for 1N4R tau with a P301S mutation, and V. Lee for GT38 antibody. **Funding:** This work was supported by National Institutes of Health 1R01AG070895 (D.S.E.), National Institutes of Health RF1AG065407 (D.S.E.), National Institutes of Health grant R01AG066212 (S.F.), National Institutes of Health grant R35 GM145286 (J.A.L.), Alzheimer's Association Research Fellowship AARF-21-848751 (K.H.), VA Merit BX004332 (G.C.), and VA Merit 1 I01 BX005919-01 (S.F.). **Author contributions:** Conceptualization: K.H. and D.S.E. Protein purification: R.A. and P.S. Nanoparticle synthesis: K.H. and M.B. In vitro and cell experiments: K.H. and J.L.D. Mouse experiments: K.H., H.P., H.S.-K., C.H., M.M., G.C., and S.F. Immunohistochemistry staining and Western blot: K.H., M.J., X.Z., S.F., and G.C. Mass spectrometry: C.L. and J.A.L. Supervision: G.C., S.F., and D.S.E. Writing—original draft: K.H. and D.S.E. Writing—review and editing: K.H., M.R.S., and D.S.E. **Competing interests:** D.S.E. is SAB chair and equity holder of ADRx Inc. All other authors declare they have no competing interests. We acknowledge our provisional patent application (Serial No. 63/510,194). **Data and materials availability:** All data needed to evaluate the conclusions in the paper are present in the paper and/or the Supplementary Materials.

Submitted 12 October 2023
Accepted 29 March 2024
Published 1 May 2024
10.1126/sciadv.adl2991